Chemical Science

ROYAL SOCIETY OF CHEMISTRY

EDGE ARTICLE

View Article Online
View Journal | View Issue

Cite this: *Chem. Sci.*, 2023, **14**, 13410

All publication charges for this article have been paid for by the Royal Society of Chemistry

Received 12th August 2023
Accepted 5th November 2023

DOI: 10.1039/d3sc04238c

rsc.li/chemical-science

Unprecedented sesterterpenoids, orientanoids A–C: discovery, bioinspired total synthesis and antitumor immunity†

Cheng-Yu Zheng,‡[ac] Jin-Xin Zhao, ‡[a] Chang-Hao Yuan,‡[acd] Xia Peng,[a] Meiyu Geng,[acd] Jing Ai,*[ac] Yao-Yue Fan*[ac] and Jian-Min Yue *[abc]

Sesterterpenoids are a very rare class of important natural products. Three new skeletal spiro sesterterpenoids, named orientanoids A–C (**1–3**), were isolated from *Hedyosmum orientale*. Their structures were determined by a combination of spectroscopic data, X-ray crystallography, and total synthesis. To obtain adequate materials for biological research, the bioinspired total syntheses of **1–3** were effectively achieved in 7–8 steps in overall yields of 2.3–6.4% from the commercially available santonin without using any protecting groups. In addition, this work also revised the stereochemistry of hedyosumins B (**6**) and C (**10**) as 11*R*-configuration. Tumor-associated macrophages (TAMs) have emerged as important therapeutic targets in cancer therapy. The in-depth biological evaluation revealed that these sesterterpenoids antagonized the protumoral and immunosuppressive functional phenotype of macrophages *in vitro*. Among them, the most potent and major compound **1** inhibited protumoral M2-like macrophages and activated cytotoxic $CD8^+$ T cells, and consequently inhibited tumor growth *in vivo*.

Introduction

Natural products (NPs) are a valuable source for the development of drugs that are of particularly high importance to modulate inflammation and immunity,[1,2] and some of the bioactive NPs often serve as handy tools for chemical biology to probe unknown biological processes and/or to identify drug targets.[3,4] Terpenoids (C_{5n} skeletons) are the largest compound class of NPs, and account for over one-third (*ca.* 110 000) of the total number of NPs identified hitherto.[5–7] Meanwhile, sesterterpenoids (C_{25}) are the smallest group (*ca.* 1000) among the terpenoid family, of which the vast majority have marine origins, and only very limited numbers have been reported from terrestrial plants.[8–13] The fascinating structures and significant bioactivities of sesterterpenoids have been attracting broad interest from many associated scientific communities.[14–19] Our preliminary studies on *Hedyosmum orientale* Merr. et Chun led to the isolation of three guaianolides, a guaiane-type sesquiterpenoid dimer, and a eudesmane–guaiane heterodimeric sesquiterpenoid.[20–22] As part of our continuing efforts for the discovery of structurally unique and biologically potent natural products from medicinal plants,[23–25] three sesterterpenoids, orientanoids A–C (**1–3**), were further identified from *H. orientale*. Compounds **1–3** possessed an unprecedented spiro carbon skeleton by incorporating the main components of a decahydro-4,7-epoxyazulene and a contiguous 2-oxaspiro[4.5]decane. Biosynthetically, compounds **1–3** could be derived from a monoterpenoid diene **4** and the coexisting guaiane sesquiterpenoid, hedyosumin A (**5**) through an intermolecular Diels–Alder reaction. To mimic the biosynthetic proposal and acquire sufficient amounts of samples for further biological study,[26,27] the bioinspired total syntheses of compounds **1–3** were thus achieved in a very concise and elegant manner without using any protecting groups.

Guaiane sesquiterpenoids, such as englerins with nanomolar anticancer activity, are an important class of biological natural products and have attracted broad interest from both chemistry and biology communities.[28,29] As the pivotal Diels–Alder precursor, compound **5** has been effectively synthesized in 13 or 14 steps.[30,31] However, a more concise synthesis of **5** remains a challenge. In the present study, a bioinspired synthesis of **5** was achieved in 6 steps from santonin involving

[a]*State Key Laboratory of Drug Research, Shanghai Institute of Materia Medica, Chinese Academy of Sciences, Shanghai 201203, China. E-mail: jai@simm.ac.cn; s040500290@126.com; jmyue@simm.ac.cn*

[b]*Research Units of Discovery of New Drug Lead Molecules, Chinese Academy of Medical Sciences, Shanghai 201203, China*

[c]*University of Chinese Academy of Science, No. 19A Yuquan Road, Beijing 100049, China*

[d]*School of Pharmaceutical Science and Technology, Hangzhou Institute for Advanced Study, University of Chinese Academy of Sciences, Hangzhou 310024, China*

† Electronic supplementary information (ESI) available. CCDC 2002618, 2002619, 2002637–2002639, 2013505, 2022064, 2022065, 2181591 and 2216319. For ESI and crystallographic data in CIF or other electronic format see DOI: https://doi.org/10.1039/d3sc04238c

‡ These authors contributed equally.

a photochemical rearrangement and a subsequent intramolecular oxa-Michael reaction as the key steps. During the synthesis course, its two biosynthetic upstream guaiane sesquiterpenoids, hedyosumins B (**6**) and C (**10**),[20] were also obtained and structurally revised as their C-11 epimers.

TAMs have been demonstrated to suppress the recruitment and function of cytotoxic T cells, promote angiogenesis, and affect multiple other aspects of tumor immunity, which together generate an immunosuppressive tumor microenvironment (TME) that finally promotes tumor growth and metastasis as well as mediating resistance to anticancer therapy.[32] Generally, in contrast to the anti-tumor M1-like macrophages, the pro-tumor macrophages appear as M2-like polarized ones.[33] It was observed that the T cell exhaustion was associated with the M2-like macrophages in the immune-rich TME.[34] Thus, TAM-centric therapy has emerged as an important strategy for cancer treatment clinically.[35,36] In a TAM-centric anticancer drug screening project, natural compounds **1–3** and their synthetic analogs showed inhibition toward the protumoral and immunosuppressive phenotype of macrophages *in vitro*. Furthermore, in the TAM-rich immunocompetent murine tumor models, the most potent and major compound **1** exhibited significant activities to remodel the TME by inhibiting protumoral M2-like macrophage infiltration and increasing activated $CD8^+$ T cell infiltration, and consequently inhibited tumor growth *in vivo*.

Herein, we present a holistic study of compounds **1–3** and/or their synthetic analogs that spans the isolation, structure elucidation, total syntheses, and biological evaluation.

Results and discussion

Isolation, structure elucidation and plausible biosynthetic consideration of 1–3

An EtOH extract prepared from the powder of the twigs and leaves of *H. orientale* was suspended in water and partitioned with EtOAc. Sequential separations of the EtOAc extract by column chromatography and semi-preparative HPLC purification afforded compounds **1–3**.

Orientanoid A (**1**), colorless crystals, has a molecular formula of $C_{25}H_{32}O_5$ with 10 double-bond equivalents (DBEs) as deduced from the HRESIMS ion at *m*/*z* 435.2145 $[M + Na]^+$ (calcd for $C_{25}H_{32}O_5Na$, 435.2147) and its ^{13}C NMR data (Table S1, ESI†). The IR spectrum displayed absorption bands for hydroxy (3470 cm^{-1}), carbonyl (1768 cm^{-1}), and olefin (1655 cm^{-1}) functionalities. The ^1H NMR data (Table S1, ESI†) showed typical proton resonances for five methyls and three olefinic methines. With the aid of DEPT and HSQC experiments, 25 carbon resonances observed in the ^{13}C NMR spectrum were distinguished as two carbonyls, three double bonds, five methyls, five sp^3 methylenes, three sp^3 methines, and four sp^3 non-proton-bearing carbons. The two carbonyls and three double bonds accounted for 5 DBEs, and the remaining ones thus required compound **1** being pentacyclic.

The 2D structure of **1** was mainly delineated by 2D NMR interpretation (Fig. S1, ESI†). Four proton-bearing fragments as drawn in bold bonds were defined by the ^1H–^1H COSY spectrum, and were then assembled with the non-proton-bearing carbons and oxygen atoms to furnish the scaffold of **1** by the HMBC spectrum. Specifically, the HMBC correlation networks of H-2 and H_3-14/C-3, C-4, and C-5; H-6/C-1, C-4, C-8, and C-7; H-8/C-12; H-13/C-11 and C-12; and H_3-15/C-1, C-9, and C-10, as well as the ^1H–^1H COSY correlations of H-1/H-2 and H-8/H-9, enabled the establishment of a guaiane-type sesquiterpenoid framework. An oxo-bridge between C-7 (δ_C 91.3) and C-10 (δ_C 86.7) was recognized by their chemical shifts to form a unique 8-oxabicyclo[3.2.1]octane moiety. The HMBC cross-peaks of H-13/C-4′; H-4′/C-7; and H-10′/C-2′, C-3′, and C-4′, along with the ^1H–^1H COSY cross-peaks of H-13/H-1′/H-2′ forged the six-membered E ring, which fused with the D-ring *via* the C-11 to shape a novel oxaspiro[4.5]decane system. The HMBC correlations of H_3-8′ (9′)/C-6′ and C-7′ (δ_C 71.1), as well as the ^1H–^1H COSY correlations of H-4′/H-5′/H-6′, constructed the C-4′ appendage of a 2-methylbut-3-en-2-ol moiety. Thus, compound **1** was elucidated to be a unique 5/6/5/5/6-pentacyclic spiro sesterterpenoid.

The relative configuration of **1** was primarily assigned using the NOESY spectrum (Fig. S1, ESI†). The NOESY correlations of H_3-15 with H-1 and H-9α revealed that these protons were cofacial, and were randomly assigned to be α-oriented. Subsequently, the NOESY correlations of H-6β with H-8 and H_3-14, as well as H-8 with H-9β indicated that they were β-oriented. The vital NOESY cross-peaks of H-6β with H-5′, and H-4′ with H-13, H-6′, and H_3-10′ fixed the orientation of the spiro E ring, as well as an E-geometry for the $\Delta^{5'}$ double bond that was consistent with the large coupling constant ($J_{5',6'}$ = 15.1 Hz). The absolute configuration of **1** was finally determined to be 1*R*, 7*S*, 8*S*, 10*R*, 11*S*, 4′*S*, 5′*E* [absolute structure parameter: 0.10(7); CCDC 2002619][37] by X-ray crystallography study with Cu Kα radiation (Fig. 1).

Orientanoid B (**2**), an amorphous white powder, shared the same molecular formula ($C_{25}H_{32}O_5$) as **1** based on the HRESIMS ion at *m*/*z* 435.2157 $[M + Na]^+$ (calcd 435.2147) and its ^{13}C NMR data (Table S1, ESI†), suggestive of isomeric analogs. The 1D NMR data of compounds **1** and **2** (Table S1, ESI†) showed high similarity with the major differences evident in the chemical shifts of C-13, C-4′, C-5′, and C-6′. Further analysis of the ^1H–^1H COSY and HMBC spectra of **2** (Fig. S2a, ESI†) indicated that its

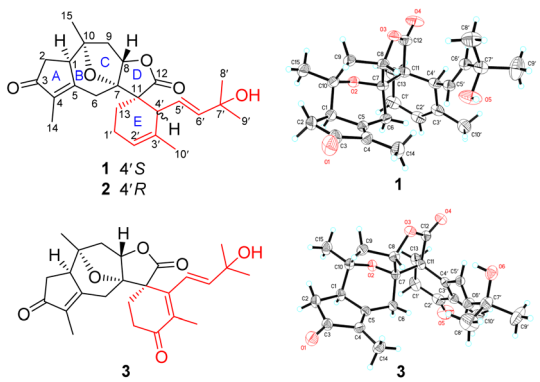

Fig. 1 The structures of compounds **1–3**.

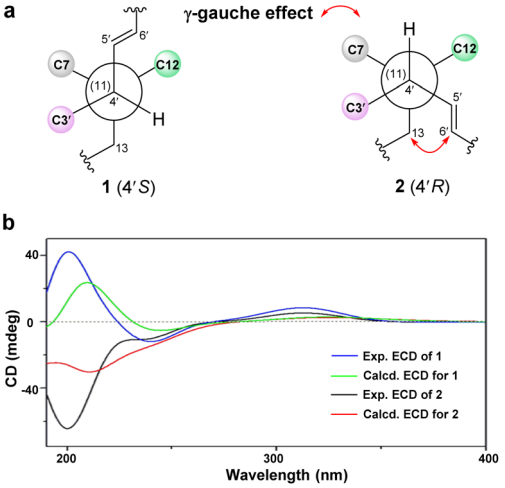

Fig. 2 (a) Newman projections along the C4′/C11 bond for **1** and **2**. (b) Experimental and calculated ECD spectra of compounds **1** and **2**.

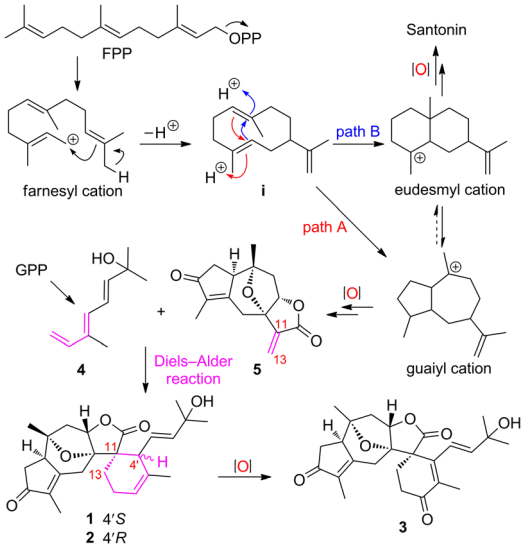

Scheme 1 Plausible biosynthetic consideration of **1–3**.

2D structure was identical to that of **1**. Examination of the NOESY spectrum (Fig. S2b, ESI†) and the key coupling constants revealed that the stereochemistry of A–D rings and the E-geometry of the $\Delta^{5'}$ double bond ($J_{5',6'} = 15.4$ Hz) in **2** were retained as those of **1**, and the only variation was likely the C-4′ configuration. This was validated by the key NOESY correlations of H-4′ with H-8 and H-6β, as well as H-13 with H-5′. Compared with compound **1**, the chemical shift of C-13 in **2** was severely resonated upfield ($\Delta\delta_C$ −6.4 ppm) due to the γ-gauche effects from the $\Delta^{5'}$ double bond (Fig. 2a). The absolute configuration of **2** was then assigned as 1*R*, 7*S*, 8*S*, 10*R*, 11*S*, 4′*R*, 5′*E* from the roughly matched experimental and calculated ECD curves (Fig. 2b).

Orientanoid C (**3**), colorless crystals, has a molecular formula of $C_{25}H_{30}O_6$ with 11 DBEs based on the HRESIMS ion at *m*/*z* 471.2018 $[M + HCO_2]^-$ (calcd 471.2019) and its ^{13}C NMR data (Table S1, ESI†), which is one oxygen atom more and two hydrogen atoms less than that of **1**, suggesting it is likely an oxidative analog of **1**. This was supported by their similar NMR data, and in particular, the ^{13}C NMR spectrum of **3** showed characteristic resonances for three carbonyls (one ester and two ketones) and three double bonds (one disubstituted and two persubstituted). Specifically, the additional ketone carbonyl (δ_C 199.5) was assigned to C-2′ by the vital HMBC correlations (Fig. S3a, ESI†) from H_2-13 and H_3-10′ to C-2′. A $\Delta^{3'}$ double bond was further located by the HMBC correlations from H_3-10′ to C-3′ (δ_C 136.7) and C-4′ (δ_C 148.2), as well as from H_2-13 to C-4′. Comprehensive 2D NMR data analysis (Fig. S3a, ESI†) showed that the A–D rings and the C-4′ appendage of **3** remained the same as those of **1** and **2**, and the only discrepancy was that the E ring of **3** was modified to a cyclohex-2-en-1-one. The NOESY correlations of H-1 with H-6α and H_3-15; H-6β with H-8 and H_3-14; H-8 with H-9β and H-5′; H_3-14 with H-10′; and H_3-15 with H-2α and H-9α (Fig. S3b, ESI†), as well as the key coupling constant ($J_{5',6'} = 16.1$ Hz) allowed the establishment of its relative configuration as depicted. The absolute configuration of **3** was finally determined to be 1*R*, 7*S*, 8*S*, 10*R*, 11*S*, 5′*E* [absolute structure parameter: −0.08(9); CCDC 2002618] by X-ray crystallographic study with Cu Kα radiation (Fig. 1).

Biosynthetically, the origins of sesterterpenoids **1–3** could be readily tracked back to the assembly of a coexisting major guaiane-type sesquiterpenoid, hedyosumin A (**5**), with a monoterpenoid (**4**) *via* an intermolecular Diels–Alder reaction (Scheme 1). The biosynthesis of guaiane-type sesquiterpenoids, *e.g.* hedyosumin A, was proposed to originate from the farnesyl cation *via* a pivotal monocyclic sesquiterpenoid intermediate **i**. The intermediate **i** *via* the path A of an acidic catalyzed annulation produced the guaiyl cation, which then underwent a cascade of oxidative modifications to yield hedyosumin A. Meanwhile, the intermediate **i** *via* an alternative path B of cyclization could generate the eudesmyl cation, which would finally produce the famous molecule of NPs, santonin.[38] This indicated that guaiane-type and eudesmane-type sesquiterpenoids have inherent connections biosynthetically, suggesting that they might be mutually transformed conditionally. This was supported by a successfully photochemical rearrangement from santonin to the guaiane-type sesquiterpenoid framework.[39–41]

Chemical synthesis of 1–3

The scarce sample amounts (1.9–3.5 mg) of compounds **1–3** have unfortunately hampered deeper investigations on these unique spirocyclic scaffolds. In order to obtain sufficient materials for further bioactivity studies, the chemical syntheses of **1–3** were implemented.

Inspired by the proposed biosynthetic pathway, the retrosynthetic stream of thought toward **1–3** (Scheme 2) materialized as follows: (1) an intermolecular Diels–Alder reaction between hedyosumin A (**5**) and a monoterpenoid (**4**) was intended to directly construct compounds **1** and **2**; (2) compound **3** was envisioned to be descended from **1** and/or **2** *via* a sequential singlet oxygen ene reaction and dehydration; (3) a thought-provoking transformation from the commercially available

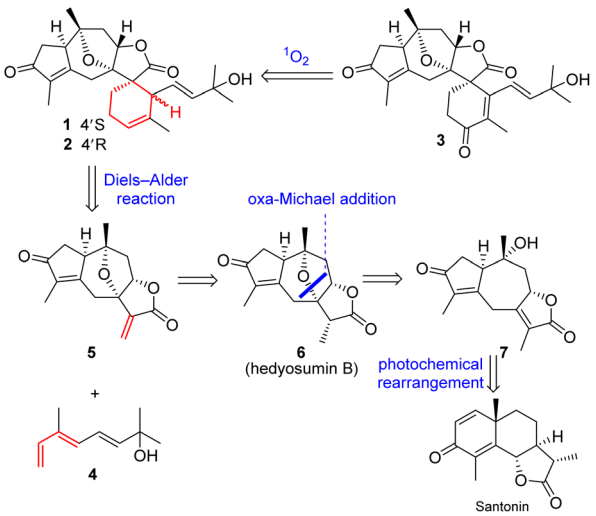

Scheme 2 Retrosynthetic analysis of **1**–**3**.

material santonin to the crucial intermediate hedyosumin A (**5**) was deliberated through several steps, in which compound **5** could be formed by a challenging direct α,β-dehydrogenation of **6** that could be forged by a intramolecular oxa-Michael addition from **7**.

The total synthesis commenced with the construction of hedyosumin A (**5**), and a six-step efficient approach to **5** in an enantioselective manner was thus developed (Scheme 3). First, the known compound **8** was made from santonin in one step according to the reported procedure.[42] Next, the allylic hydroxylation of enone **8** proved challenging. After screening various reaction conditions (Table S15, ESI†), enone **8** was successfully hydroxylated to provide **9** in 30% yield by employing the enone oxidation method developed by us quite recently.[43] The structure of **9** was confirmed by single crystal X-ray diffraction [absolute structure parameter: −0.07(9); CCDC 2216319]. Having secured compound **9**, the photochemical rearrangement/lactonization/alkene migration cascade reaction[40] was achieved to give the desired **7** in 90% yield by irradiating a solution of **9** in AcOH/H_2O,[44] with 365 nm LEDs (50 W). Then our effort was focused on the installation of the 7,10-epoxy bridge to produce hedyosumin B (**6**) *via* the intramolecular oxa-Michael addition. After a brief survey of the reaction conditions (Table S17, ESI†), we were delighted to find that upon treatment with $NaHCO_3$ in dioxane/H_2O at room temperature, compound **7** smoothly underwent oxa-Michael addition to afford product **6** as a single diastereomer in 72% yield. The stereospecificity is attributable to the strong stereochemical bias of the substrate. The absolute structure of **6** was determined as depicted by single crystal X-ray diffraction [absolute structure parameter: −0.05(6); CCDC 2002637], which is actually the C-11 epimer of hedyosumin B. However, its spectroscopic data and physical constants well matched those of the latter, and allowed the revision of the structure of hedyosumin B as **6**. With the key intermediate **6** in hand, we carried out direct oxidative dehydrogenation of **6** under various conditions with different oxidants, such as DDQ and IBX, aiming to generate the exocyclic double bond of **5**, which was proved to be unsuccessful and the starting material was kept unreacted in all the cases. As an alternative, the reduction of **6** with $NaBH_4$ in MeOH provided an

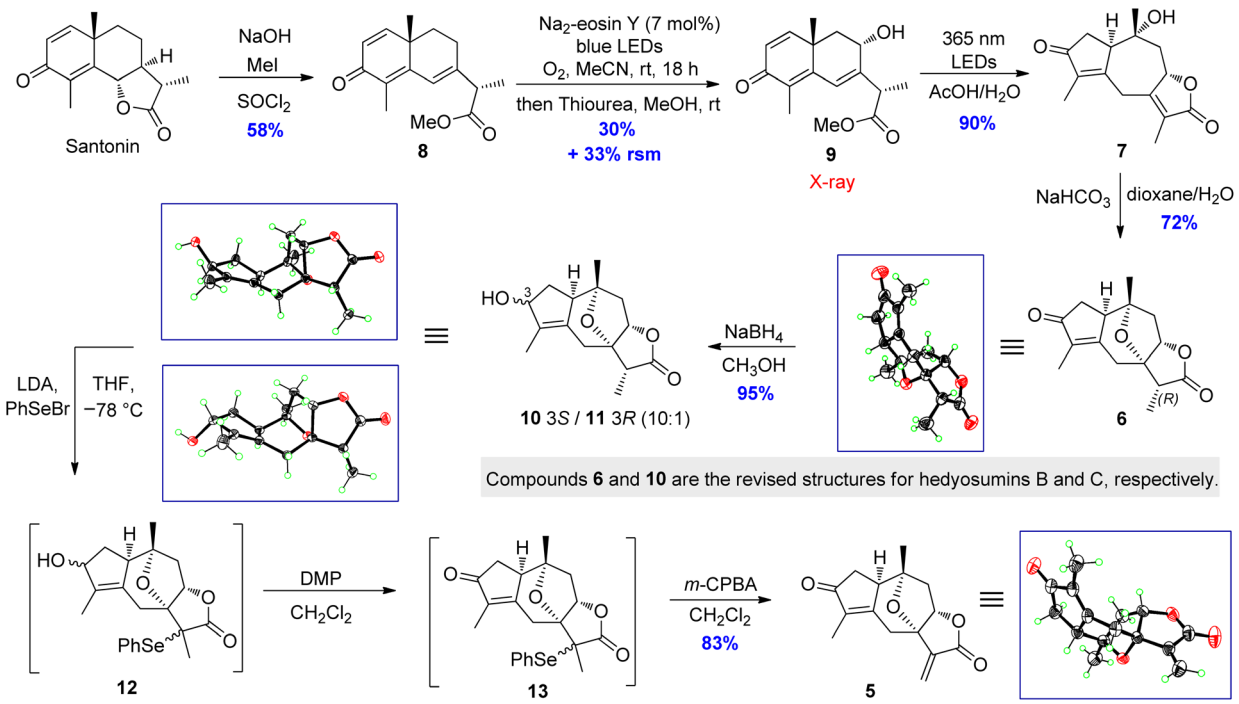

Scheme 3 Synthesis of key intermediate hedyosumin A (**5**). LED = light-emitting diode; RSM = recovered starting material; LDA = lithium diisopropylamide; Ph = phenyl; DMP = Dess–Martin periodinane; *m*-CPBA = *meta*-chloroperoxybenzoic acid.

epimeric mixture of compound **10** and its C-3 epimer **11** (10 : 1) in 95% combined yield. The absolute structures of **10** and **11** were confirmed by single crystal X-ray diffraction [**10**: absolute structure parameter: −0.08(11); CCDC 2022064. **11**: absolute structure parameter: 0.03(4); CCDC 2022065]. Similarly, the structure of hedyosumin C was revised to be **10** by comparing the spectroscopic data of the NP and the synthetic counterpart, as well as the correlation of this chemical transformation. To our delight, a very effective dehydrogenation of **10** and its C-3 epimer was exploited to yield dienophile **5** in a one-pot reaction and protecting-group-free manner. Briefly, the mixture of **10** and its C-3 epimer was treated with LDA in THF, and the resultant enolates were then reacted with PhSeBr to give the corresponding mixture of selenylated lactones, which were finally subjected to a Dess–Martin oxidation and subsequent *m*-CPBA-mediated oxidative elimination[45] to give compound **5** in 83% yield in one pot. Compound **5** was verified to be hedyosumin A by X-ray diffraction analysis [absolute structure parameter: 0.09(8); CCDC 2002638].

The monoterpenoid, octa-3(*E*),5(*E*)-trien-2-ol (**4**), was synthesized from the commercially available ethyl (*E*)-3-methyl-4-oxo-2-butenoate in 6 steps according to the literature procedures.[46,47] With both diene **4** and dienophile **5** in hand, we next explored the intermolecular Diels–Alder reaction (Scheme 4). After several attempts, the desired products of orientanoids A (**1**, Si-*exo*) and B (**2**, Si-*endo*), as well as two undesired minor compounds **14** (Re-*exo*) and **15** (Re-*endo*) were obtained in 81% combined yield by heating the mixture of compounds **4** and **5** in a neat form at 80 °C for 18 h without any catalysts. In this operation, the neat mixture of **4** and **5** was well managed in thin film and foiled to the reaction flask. This is a regio-specific Diels–Alder reaction, in which four expected products as mentioned above were produced and no other positional isomers were detected. The structures of the synthetic orientanoid A and **14** were confirmed by X-ray diffraction analysis [**1**: absolute structure parameter: −0.03(10); CCDC 2002639. **14**: absolute structure parameter: 0.08(7); CCDC 2181591], and the structures with absolute configurations of the synthetic compounds **2** and **15** were assigned by extensive spectroscopic analysis and ECD calculation (Fig. S5 and S6, ESI†). With synthetic minor isomers **14** and **15** in hand, we performed LC-MS analysis of crude extracts of the title plant. Based on the LC-MS analysis reports (pages 106–111 in the ESI†), we propose that compounds **14** and **15** may also be natural products, which were likely lost in the processes of isolation and/or purification due to their much lower concentrations.

The *endo* products of Diels–Alder addition are normally preferred when the electron-withdrawing groups, such as carbonyl, are conjugated with the dienophile owing to the following secondary orbital interactions. However, in the current study, despite a carbonyl group being conjugated to the dienophile, the *exo* products were abnormally predominant in the resultant reaction. The unexpected ratios of *endo* and *exo* products attracted our great interest in seeking the immanent mechanism. Four plausible transition states **a–d** for compounds **1**, **2**, **14** and **15** in the Diels–Alder reaction were proposed as depicted in Fig. 3, respectively. The products (**1** and **2**) yielded by the diene reaching from the Si-face (referring to the C-12 carbonyl group) of dienophile **5** were much more abundant than those (**14** and **15**) formed *via* the Re-face addition due largely to the presence of steric hindrances from the 7,10-epoxy bridge in the transition states **c** and **d**. Meanwhile, the yields of *exo* adducts (**1** and **14**) were unusually higher than those of *endo* ones (**2** and **15**) owing to the balanced net dipole moments between the dienophile enone system and diene in the *exo* cases

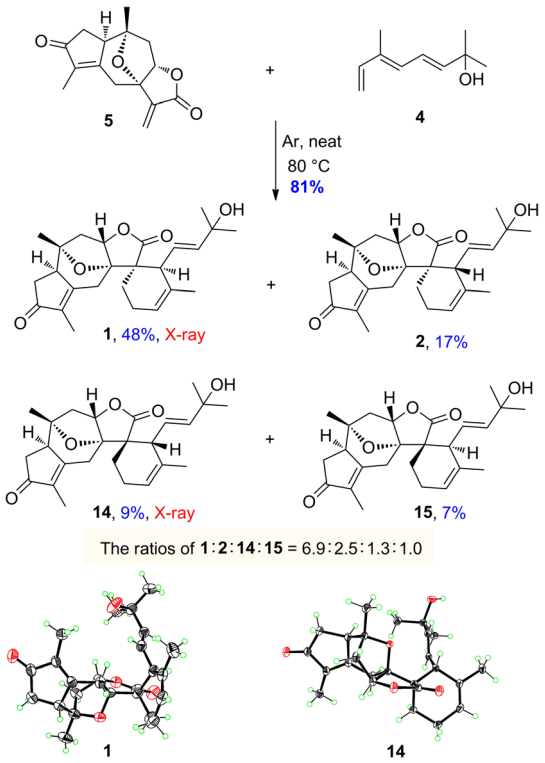

Scheme 4 Syntheses of orientanoids A (**1**) and B (**2**).

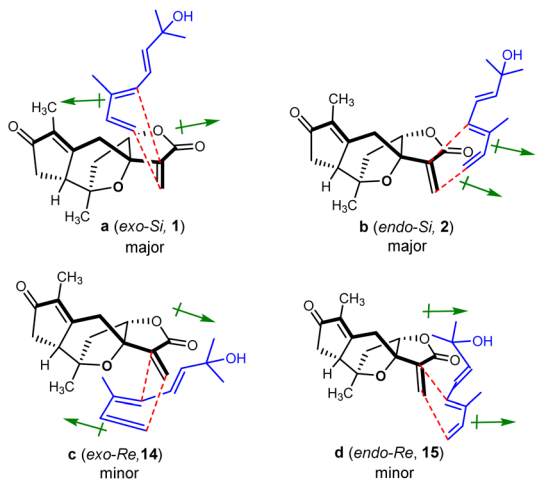

Fig. 3 Transition states proposed for the regio-specific intermolecular Diels–Alder reactions of **4** and **5** (↦: denotes dipole moments of the dienophile enone and diene systems).

being smaller than those in the *endo* ones, resulting in the relatively lower free energy for the *exo* transition states.[48–50] The total stability for each of the transition states **a–d** was regulated by both the steric effects and the net balanced dipole moments, which finally determined the yields of the products. In recent years, various bimolecular stereoselective Diels–Alderases in nature have been discovered,[51,52] so it is also possible that **1** and **2** are selectively formed due to enzyme-dependent [4 + 2] cycloaddition in the biogenetic pathway, which needs further verification.

According to the biosynthetic proposal (Scheme 1), we believed that orientanoid C is the more downstream metabolite that might be derived from orientanoids A and/or B *via* oxidative modifications. Therefore, after completing the syntheses of orientanoids A and B, we directed our focus to make orientanoid C from the synthetic formers *via* the initiative of oxidative modifications.

After enormous efforts, we finally focused on the singlet oxygen ene reaction aiming to furnish the enone functionality in orientanoid C (**3**). After extensive optimization, we found that irradiating an oxygen-bubbled solution of compound **1** and methylene blue in MeCN with a 23 W fluorescent lamp at room temperature smoothly produced the expected key intermediate hydroperoxide, which was then immediately exposed to 2-iodoxybenzoic acid (IBX)[53] to afford the desired compound **3** in 72% yield in a one-pot manner (Scheme 5a).

The structure of the synthetic orientanoid C was verified by X-ray diffraction study [absolute structure parameter: −0.02(4); CCDC 2013505]. Meanwhile, orientanoid B (**2**) could not be transformed into orientanoid C (**3**) under the same conditions.

The cause of this stereo specific transformation was likely the conformational difference between two key reaction intermediates of **1** and **2**.[54,55] As depicted in Scheme 5b, the allylic hydrogen H-4′ of **1** is perfectly perpendicular to the $\Delta^{2'}$ double bond (see the X-ray structure), which is spatially conducive to form the key intermediate **1a** required for the singlet oxygen ene reaction. Meanwhile, the H-4′ of **2** is almost parallel to the $\Delta^{2'}$ double bond, which resulted in the facts that the corresponding key intermediate **2a** doesn't meet the conformational requirements for the singlet oxygen ene reaction, and is also likely unstable.

Antitumor immunity by antagonizing TAMs

With adequate quantity of compounds **1–3** and synthetic analogs in hand, we explored the effects of these compounds on the protumor phenotype of macrophages. In this test, the classic mouse monocyte-macrophages leukemia cell line RAW 264.7 was stimulated with IL-4/IL-13 to obtain M2-like protumoral phenotype macrophages, in which the mRNA expression levels of two molecules, namely MRC1 (CD206),[56] a typical M2-type marker, and ARG1,[56] a key functional effector to mediate T cells suppression, were observed to be significantly increased. The addition of compounds **1–3**, **5**, and **10** effectively inhibited this up-regulation (Fig. 4a and b) without obvious influence on cell viability (Fig. S7a, ESI†). Among them, compound **1** was found to be the most potent one and was thus selected for further evaluation both *in vitro* and *in vivo*.

We subsequently tested the inhibitory effects of compound **1** at multiple concentrations on the mRNA expression level of

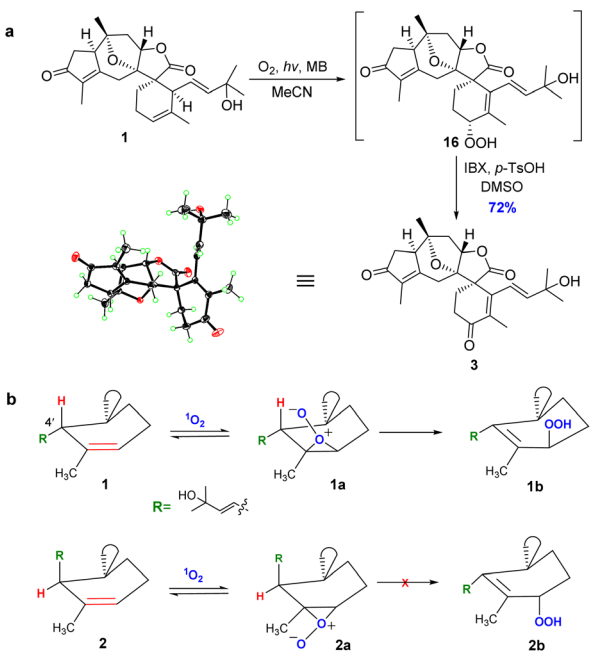

Scheme 5 (a) Synthesis of orientanoid C (**3**). MB = methylene blue; IBX = 2-iodoxybenzoic acid; *p*-TsOH = *p*-toluenesulfonic acid; DMSO = dimethylsulfoxide. (b) Stereoselectivity for the singlet oxygen ene reaction of compounds **1** and **2**.

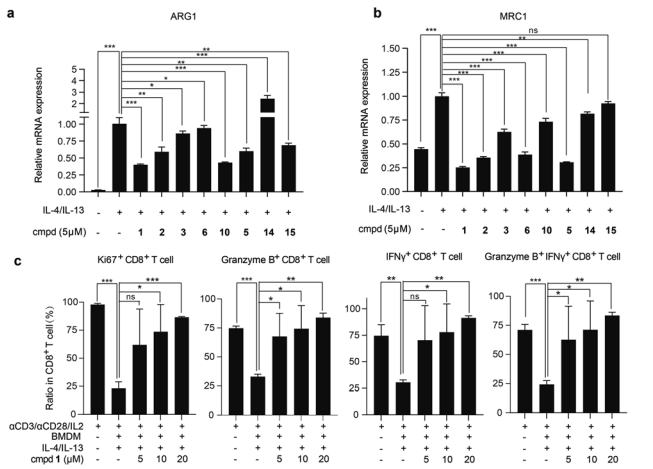

Fig. 4 The effects of compounds on the protumor phenotype and immunosuppressive function of macrophages *in vitro*. (a and b) Quantitative RT-PCR analysis for mRNA levels of ARG1 (a) and MRC1 (b) in RAW 264.7 cells treated with IL-4/IL-13 alone or combined with indicated compounds for 12 h. (c) Compound **1** reverses macrophage-mediated $CD8^+$ T suppression. BMDMs were treated with IL-4/IL-13 alone or combined with compound **1** for 48 h, followed by coculturing with spleen cells that were stimulated with anti-CD3/CD28 beads and IL-2 for 72 h. The ratio of the indicated $CD8^+$ T cell subpopulation was assessed by flow cytometry. Data represent mean ± SD from triplicates. $^*P < 0.05$, $^{**}P < 0.01$, $^{***}P < 0.001$, ns, $P > 0.05$, determined by Student's *t*-test.

ARG1, MRC1, and another classic M2-marker CD163 (ref. [57]) in IL-4/IL-13-induced RAW 264.7 cells and primary murine macrophages derived from bone marrow (BMDMs), respectively. Compound **1** dose-dependently inhibited the mRNA expression levels of ARG1, MRC1, and CD163 in both cells (Fig. S7c and d, ESI†), with no significant influence on cell viability (Fig. S7a and b, ESI†), further confirming that compound **1** suppressed the immunosuppressive and M2-polarized phenotype of macrophages. Protumoral M2-like TAMs have been demonstrated to directly suppress the proliferation and activation of $CD8^+$ T cells.[35,58] When co-cultured with autologous spleen cells, as expected, the IL-4/IL-13-induced BMDMs suppressed the proliferation and activation of $CD8^+$ T cells. Interestingly, the suppression was reversed by the pretreatment of BMDMs with compound **1**, as evidenced by a significant increase in the proportion of $Ki67^+$, granzyme B^+, and $IFN\gamma^+$, as well as granzyme B^+ $IFN\gamma^+$ $CD8^+$ T cells in total $CD8^+$ T cells (Fig. 4c). The above data indicated that compound **1** reversed the suppression of T cell proliferation and activation induced by protumoral macrophages.

Finally, we investigated the *in vivo* antitumor efficacy of compound **1** in immune-competent and nude mice, respectively (Fig. 5a and b and S8a, ESI†). In subcutaneous E0771 (ref. [59]) and Hepa1-6 (ref. [60]) immunocompetent murine tumor models with abundant macrophages, compound **1** consistently and significantly delayed tumor growth (Fig. 5a and S8a, ESI†) at well-tolerated doses (Fig. S8b and c, ESI†). Concurrently, the infiltration of macrophages and $CD8^+$ T cells in tumor tissue of the representative murine E0771 model was analyzed, which indicated that compound **1** notably reduced the infiltration of protumoral M2-like $CD206^+$ macrophages and increased the infiltration of $IFN\gamma^+$ and $TNF\alpha^+$ $CD8^+$ T cells (Fig. 5c) without significant impact on the infiltration of total immune cells, macrophages and $CD8^+$ T cells (Fig. S8e, ESI†). We also established the Hepa1-6 subcutaneous nude mouse tumor model, which lacks T cells, the key target cell suppressed by TAMs. By contrast, the antitumor effect of compound **1** was apparently greatly attenuated in nude mice (Fig. 5b). Additionally, compound **1** exhibited no significant inhibition on the cell viability of Hepa1-6 and E0771 cells *in vitro* (Fig. S9, ESI†). The above evidence suggested that compound **1** exerted antitumor effects *in vivo* mainly by suppressing protumoral macrophages and activating antitumoral $CD8^+$ T cells, rather than through a direct cytotoxic effect on tumor cells.

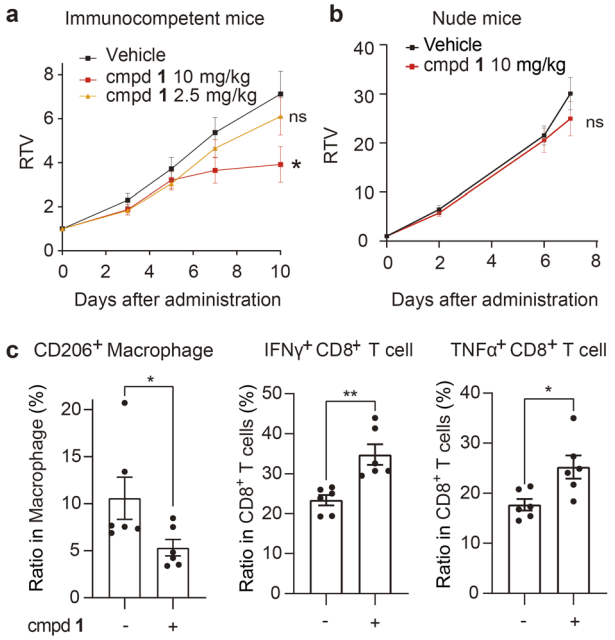

Fig. 5 Compound **1** reshapes the tumor immune microenvironment and inhibits tumor growth *in vivo*. (a and b) Immune-competent mice bearing Hepa1-6 xenograft ($n = 11$ per group) (a) or nude mice bearing Hepa1-6 xenograft ($n = 10$ per group) (b) were intratumorally administered with compound **1** or the vehicle daily for the indicated period. The relative tumor volume (RTV) is shown as the mean ± SEM. (c) Flow cytometric analysis of tumor infiltrated immune cell subsets in the E0771 tumor model treated with compound **1** (5 mg kg^{-1}) ($n = 6$ per group). See details in the ESI.† Data are shown as the mean ± SEM. $^*P < 0.05$, $^{**}P < 0.01$, ns $P > 0.05$ *vs.* the vehicle group, determined by Student's *t*-test.

Conclusions

In summary, three unprecedented sesterterpenoids (**1–3**) were isolated and structurally characterized from *H. orientale*. Further to this, the concise and asymmetric syntheses of compounds **1–3** were accomplished in 7–8 steps with overall yields of 2.3–6.4% starting from the commercially available santonin without using any protecting groups, which not only corroborated the structural assignments but also imitated the biosynthetic proposal for these sesterterpenoids. Chemically, it is notable that a concise access to the guaiane-type sesquiterpenoids, such as hedyosumins A–C, was exploited involving a photochemical rearrangement of a santonin derivative as the key step, and a highly robust and catalyst-free intermolecular Diels–Alder reaction was accomplished to afford the desired products under very mild conditions by managing two reaction substrates in a well-mixed film of neat form. Biologically, this sesterterpenoid class, *e.g.* compound **1**, inhibited tumor growth by reshaping the TME *via* antagonizing TAMs and activating antitumor immunity. The unprecedented structures and the unique anticancer mechanism of these rare sesterterpenoids provided a new class of drug leads for TAM-centric cancer therapy.

Data availability

General information, detailed experimental procedures, and characterization data for all new compounds can be found in the ESI.†

Author contributions

Y. Y. F. performed the isolation and structural elucidation of natural compounds. C. Y. Z. and J. X. Z. performed the biomimetic syntheses. C. H. Y., X. P., M. G., and J. A. contributed to the bioactive evaluation. J. M. Y. designed and supervised the

project, and edited the manuscript. All authors discussed the results and commented on the manuscript.

Conflicts of interest

There are no conflicts to declare.

Acknowledgements

This work was financially supported by the National Natural Science Foundation (22237007, 81821005, and 82122062) of the People's Republic of China, the CAMS Innovation Fund for Medical Sciences (2019-I2M-5-080), the CAS Biological Resources Program (KFJ-BRP-008), the Collaborative Innovation Cluster Project of Shanghai Municipal Commission of Health and Family Planning (No. 2020CXJQ02), and the Shanghai Municipal Science and Technology Major Project. We also thank Prof. S.-M. Huang of Hainan University for the identification of the plant material.

Notes and references

1 A. F. Majdalawieh and M. W. Fayyad, *Int. Immunopharmacol.*, 2015, **28**, 295–304.
2 M. Yin, Y. Zhang and H. Li, *Front. Immunol.*, 2019, **10**, 145.
3 B. J. Huffman and R. A. Shenvi, *J. Am. Chem. Soc.*, 2019, **141**, 3332–3346.
4 J. W. H. Li and J. C. Vederas, *Science*, 2009, **325**, 161–165.
5 T. Zeng, Z. Liu, J. Zhuang, Y. Jiang, W. He, H. Diao, N. Lv, Y. Jian, D. Liang, Y. Qiu, R. Zhang, F. Zhang, X. Tang and R. Wu, *J. Chem. Inf. Model.*, 2020, **60**, 2082–2090.
6 D. W. Christianson, *Chem. Rev.*, 2017, **117**, 11570–11648.
7 D. Tholl, *Adv. Biochem. Eng./Biotechnol.*, 2015, **148**, 63–106.
8 K. Li and K. R. Gustafson, *Nat. Prod. Rep.*, 2021, **38**, 1251–1281.
9 K. Guo, Y. Liu and S. H. Li, *Nat. Prod. Rep.*, 2021, **38**, 2293–2314.
10 P. Máximo and A. Lourenço, *Curr. Org. Chem.*, 2018, **22**, 2381–2393.
11 L. Wang, B. Yang, X.-P. Lin, X.-F. Zhou and Y. Liu, *Nat. Prod. Rep.*, 2013, **30**, 455–473.
12 Y. Liu, L. Wang, J. H. Jung and S. Zhang, *Nat. Prod. Rep.*, 2007, **24**, 1401–1429.
13 J. R. Hanson, *Nat. Prod. Rep.*, 1996, **13**, 529–535.
14 M. Liu, W. Sun, L. Shen, Y. He, J. Liu, J. Wang, Z. Hu and Y. Zhang, *Angew. Chem., Int. Ed.*, 2019, **58**, 12091–12095.
15 C. Yuan, B. Du, L. Yang and B. Liu, *J. Am. Chem. Soc.*, 2013, **135**, 9291–9294.
16 D. Q. Thach, Z. G. Brill, H. K. Grover, K. V. Esguerra, J. K. Thompson and T. J. Maimone, *Angew. Chem., Int. Ed.*, 2020, **59**, 1532–1536.
17 N. Zhao, S. Yin, S. Xie, H. Yan, P. Ren, G. Chen, F. Chen and J. Xu, *Angew. Chem., Int. Ed.*, 2018, **57**, 3386–3390.
18 Z. G. Brill, H. K. Grover and T. J. Maimone, *Science*, 2016, **352**, 1078–1082.
19 C. L. Hugelshofer and T. Magauer, *J. Am. Chem. Soc.*, 2015, **137**, 3807–3810.
20 Z.-S. Su, S. Yin, Z.-W. Zhou, Y. Wu, J. Ding and J.-M. Yue, *J. Nat. Prod.*, 2008, **71**, 1410–1413.
21 Y.-Y. Fan, Y.-L. Sun, B. Zhou, J.-X. Zhao, L. Sheng, J.-Y. Li and J.-M. Yue, *Org. Lett.*, 2018, **20**, 5435–5438.
22 Y.-Y. Fan, L.-S. Gan, S.-X. Chen, Q. Gong, H.-Y. Zhang and J.-M. Yue, *J. Org. Chem.*, 2021, **86**, 11277–11283.
23 C.-P. Liu, C.-Y. Xie, J.-X. Zhao, K.-L. Ji, X.-X. Lei, H. Sun, L.-G. Lou and J.-M. Yue, *J. Am. Chem. Soc.*, 2019, **141**, 6812–6816.
24 Y.-Z. Ge, B. Zhou, R.-X. Xiao, X.-J. Yuan, H. Zhou, Y.-C. Xu, M. A. Wainberg, Y.-S. Han and J.-M. Yue, *Sci. China: Chem.*, 2018, **61**, 1430–1439.
25 Y.-Y. Fan, H. Zhang, Y. Zhou, H.-B. Liu, W. Tang, B. Zhou, J.-P. Zuo and J.-M. Yue, *J. Am. Chem. Soc.*, 2015, **137**, 138–141.
26 J.-X. Zhao, Y.-Y. Yu, S.-S. Wang, S.-L. Huang, Y. Shen, X.-H. Gao, L. Sheng, J.-Y. Li, Y. Leng, J. Li and J.-M. Yue, *J. Am. Chem. Soc.*, 2018, **140**, 2485–2492.
27 B. Zhang, Y. Wang, S.-P. Yang, Y. Zhou, W.-B. Wu, W. Tang, J.-P. Zuo, Y. Li and J.-M. Yue, *J. Am. Chem. Soc.*, 2012, **134**, 20605–20608.
28 R. A. Fernandes, S. Moharana and G. N. Khatun, *Org. Biomol. Chem.*, 2023, **21**, 6652–6670.
29 Z. Wu, S. Zhao, D. M. Fash, Z. Li, W. J. Chain and J. A. Beutler, *J. Nat. Prod.*, 2017, **80**, 771–781.
30 W.-B. Sun, X. Wang, B.-F. Sun, J.-P. Zou and G.-Q. Lin, *Org. Lett.*, 2016, **18**, 1219–1221.
31 K.-Y. Wang, Y. Li, S.-L. Zhang, J.-H. Chen and Z. Yang, *Tetrahedron Lett.*, 2022, **102**, 153946.
32 D. DeNardo and B. Ruffell, *Nat. Rev. Immunol.*, 2019, **19**, 369–382.
33 A. Mantovani, F. Marchesi, A. Malesci, L. Laghi and P. Allavena, *Nat. Rev. Clin. Oncol.*, 2017, **14**, 399–416.
34 A. Combes, B. Samad, J. Tsui, N. Chew, P. Yan, G. Reeder, D. Kushnoor, A. Shen, B. Davidson, A. Barczak, M. Adkisson, A. Edwards, M. Naser, K. Barry, T. Courau, T. Hammoudi, R. Argüello, A. Rao, A. Olshen, C. Cai, J. Zhan, K. Davis, R. Kelley, J. Chapman, C. Atreya, A. Patel, A. Daud, P. Ha, A. Diaz, J. Kratz, E. Collisson, G. Fragiadakis, D. Erle, A. Boissonnas, S. Asthana, V. Chan and M. Krummel, *Cell*, 2022, **185**, 184–203.
35 A. Mantovani, P. Allavena, F. Marchesi and C. Garlanda, *Nat. Rev. Drug Discovery*, 2022, **21**, 799–820.
36 M. Pittet, O. Michielin and D. Migliorini, *Nat. Rev. Clin. Oncol.*, 2022, **19**, 402–421.
37 H. D. Flack and G. Bernardinelli, *Chirality*, 2008, **20**, 681–690.
38 P. M. Dewick, *Medicinal Natural Products: A Biosynthetic Approach*, John Wiley & Sons, Ltd, Chichester, 3rd edn, 2009, p. 212.
39 D. H. R. Barton, P. de Mayo and M. Shafiq, *J. Chem. Soc.*, 1957, 929–935.
40 G. Blay, V. Bargues, L. Cardona, B. García and J. R. Pedro, *J. Org. Chem.*, 2000, **65**, 6703–6707.
41 L. Zhang, X. Dai, L. Tao, C. Xie, M. Zhang and M. Wang, *Chin. J. Chem.*, 2017, **35**, 1284–1288.
42 G. Blay, M. Luz Cardona, B. Garcia and J. R. Pedro, *J. Org. Chem.*, 1991, **56**, 6172–6175.

43 C.-Y. Zheng and J.-M. Yue, *Nat. Commun.*, 2023, **14**, 2399.
44 F. A. Macías, A. Santana, A. Yamahata, R. M. Varela, F. R. Fronczek and J. M. G. Molinillo, *J. Nat. Prod.*, 2012, **75**, 1967–1973.
45 J. Li, W. Zhang, F. Zhang, Y. Chen and A. Li, *J. Am. Chem. Soc.*, 2017, **139**, 14893–14896.
46 S. Yildizhan and S. Schulz, *Synlett*, 2011, **2011**, 2831–2833.
47 G. Majetich, Y. Wang, Y. Li, J. K. Vohs and G. H. Robinson, *Org. Lett.*, 2003, **5**, 3847–3850.
48 F. Fotiadu, F. Michel and G. Buono, *Tetrahedron Lett.*, 1990, **31**, 4863–4866.
49 K. Takeda, I. Imaoka and E. Yoshii, *Tetrahedron*, 1994, **50**, 10839–10848.
50 W. J. Lording, T. Fallon, M. S. Sherburn and M. N. Paddon-Row, *Chem. Sci.*, 2020, **11**, 11915–11926.
51 L. Gao, C. Su, X. Du, R. Wang, S. Chen, Y. Zhou, C. Liu, X. Liu, R. Tian, L. Zhang, K. Xie, S. Chen, Q. Guo, L. Guo, Y. Hano, M. Shimazaki, A. Minami, H. Oikawa, N. Huang, K. N. Houk, L. Huang, J. Dai and X. Lei, *Nat. Chem.*, 2020, **12**, 620–628.
52 L. Gao, Y. Zou, X. Liu, J. Yang, X. Du, J. Wang, X. Yu, J. Fan, M. Jiang, Y. Li, K. N. Houk and X. Lei, *Nat. Catal.*, 2021, **4**, 1059–1069.
53 T. Kuga, Y. Sasano and Y. Iwabuchi, *Chem. Commun.*, 2018, **54**, 798–801.
54 M. Orfanopoulos, I. Smonou and C. S. Foote, *J. Am. Chem. Soc.*, 1990, **112**, 3607–3614.
55 E. L. Clennan, in *Synthetic Organic Photochemistry*, ed. A. G. Griesbeck and J. Mattay, Marcel Dekker, New York, 2005, pp. 365–390.
56 X. Li, R. Liu, X. Su, Y. Pan, X. Han, C. Shao and Y. Shi, *Mol. Cancer*, 2019, **18**, 177.
57 Y. Wang, Y. Lin, S. Qiao, J. Wang and H. Wang, *Adv. Biosyst.*, 2019, **3**, e1800232.
58 E. Peranzoni, J. Lemoine, L. Vimeux, V. Feuillet, S. Barrin, C. Kantari-Mimoun, N. Bercovici, M. Guérin, J. Biton, H. Ouakrim, F. Régnier, A. Lupo, M. Alifano, D. Damotte and E. Donnadieu, *Proc. Natl. Acad. Sci. U.S.A.*, 2018, **115**, E4041–E4050.
59 T. Muliaditan, J. Caron, M. Okesola, J. Opzoomer, P. Kosti, M. Georgouli, P. Gordon, S. Lall, D. Kuzeva, L. Pedro, J. Shields, C. Gillett, S. Diebold, V. Sanz-Moreno, T. Ng, E. Hoste and J. Arnold, *Nat. Commun.*, 2018, **9**, 2951.
60 T. Kimura, Y. Kato, Y. Ozawa, K. Kodama, J. Ito, K. Ichikawa, K. Yamada, Y. Hori, K. Tabata, K. Takase, J. Matsui, Y. Funahashi and K. Nomoto, *Cancer Sci.*, 2018, **109**, 3993–4002.